Magnetic correlations of a doped and frustrated Hubbard model: benchmarking the two-particle self-consistent theory against a quantum simulator

Guan-Hua Huang¹ and Zhigang Wu^{2,*}

¹Hefei National Laboratory, Hefei 230088, China

Recently a quantum simulator for the 2D Fermi-Hubbard model on an anisotropic triangular lattice has been realized, where both geometrical frustration and doping can be continuously tuned. Here we provide a comprehensive comparison between the magnetic correlations calculated by the two-particle self-consistent (TPSC) theory and those measured in this quantum simulator, at temperatures comparable to the spin exchange energy and Hubbard interactions comparable to the bandwidth. We find overall excellent agreements between the TPSC calculations and the measurements from the quantum simulator at all levels of frustration and doping. This is quite remarkable considering that the Hubbard model is already in the intermediate to strong coupling regime, for which very few methods yield reliable results. Our work showcases the potential of TPSC as a theoretical approach capable of providing reasonably accurate descriptions of the Hubbard model even at fairly strong interactions and when the frustration is present.

Introduction.—Quantum simulation of the 2D Fermi-Hubbard model with ultracold atomic gases has seen tremendous progress in the past decade [1–3]. These systems have long been known to offer a pristine realization of the Hubbard model through the use of optical lattices, where all the model parameters can be precisely tuned [4]; but it is the advent of quantum gas microscope with its unprecedented power of resolution [5, 6], combined with innovative ideas of cooling [7, 8], that has made simulating strongly correlated regimes possible. By now experiments have successfully reached temperatures as low as half of the spin exchange energy and along the way simulated many equilibrium and non-equilibrium properties of the Hubbard model. Among other things, these include demonstration of metal-to-insulator transition [9], probe of short- and long-range antiferromagnetic correlations [10-14], measurement of equation of state [15, 16] and study of magnetic polarons [17–19]. In addition, various transport measurements have also been carried out in the quantum simulator, such as charge transport in the bad metallic regime [20], spin transport of the Mott insulator [21] as well as subdiffusion and heat transport in the high temperature regime [22]. All these developments are encouraging signs that the ultimate goal of simulating the 2D Hubbard model at temperatures and dopings relevant to the physics of high Tc superconductivity may finally be within reach.

However, the value of a quantum simulator lies not only in revealing the properties of simulated models in regimes not accessible by classical computation tools, but also in serving as an important platform for testing various theoretical ideas used to unravel these models. For the 2D Fermi-Hubbard model, an extraordinary amount of effort has been devoted to its understanding [23] and various theoretical methods have been

proposed for its quantitative description [24, 25]. The so-called two-particle self-consistent theory (TPSC), developed by Vilk and Tremblay [26, 27], is one of such methods. TPSC is a non-perturbative approach which satisfies the Mermin-Wagner theorem, the Pauli principle and various conservation and sum rules for the charge and spin. It has been applied to a wide range of problems related to the 2D Fermi-Hubbard model [28–44] and was found to agree with Monte Carlo simulations on the calculation of various physical quantities in the weak-to-intermediate coupling regime [27], including the double occupancy, spin and charge structure factors, and single-particle spectral functions. More importantly, it predicts the opening of pseudogap [26] and the existence of d-wave superconductivity in the model [30], two very consequential results. Although calculations based on TPSC have been directly compared to measurements of cuprate superconductors [31–33], the agreement or lack thereof should be viewed along with the fact the singleband Hubbard model cannot possibly capture the real materials perfectly. For this reason, it is important to benchmark the methods proposed to solve the Hubbard model, such as the TPSC, against a quantum simulator of the model.

In this letter, we perform such a benchmarking for the first time by comparing the magnetic correlations calculated by TPSC to those measured in the quantum simulator of the doped and frustrated Hubbard model on an anisotropic triangular lattice [14]. To our surprise, we find that even for Hubbard interactions comparable to or slightly larger than the bandwidth, TPSC still gives a fairly accurate account of the magnetic correlations at almost all levels of doping and frustration. Our results highlight the capacity of TPSC in understanding strongly-correlated regimes of the Hubbard model that very few approaches can access. Within quantum simulation our work also suggests a new avenue of using quantum simulators to systematically benchmark theoretical approaches on strongly correlated models.

² Quantum Science Center of Guangdong-Hong Kong-Macao Greater Bay Area (Guangdong), Shenzhen 508045, China (Dated: September 6, 2024)

^{*} atticuspku@gmail.com

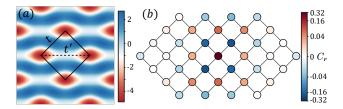


FIG. 1. (a) Optical lattice potential used in Ref. [14] to realize the quantum simulator of a tunable frustrated Hubbard model. (b) A sample of the measured real-space magnetic correlation in the quantum simulator of Ref. [14]. Here $t^{\prime}/t=0.57, \, {\rm T/t}=0.34$ and U/t=8.2.

Quantum simulator of a frustrated Hubbard model.— In the quantum simulator [14], a two-component Fermi gas is loaded into a non-separable square optical lattice potential, formed by the interference pattern of two laser beams. When the intensities of the two beams are equal, this setup realizes the standard Hubbard model on a square lattice with nearest-neighbor hopping t and onsite interaction U. Through varying the relative intensity of the two beams, the horizontal diagonal hopping t' can be tuned from zero to t continuously, thereby realizing a tunable triangular lattice potential (see Fig. 1(a)). The Hamiltonian of the Hubbard model on such a lattice reads

$$\hat{H} = -t \sum_{\langle ij \rangle \sigma} \hat{c}_{i\sigma}^{\dagger} \hat{c}_{j\sigma} - t' \sum_{\langle \langle ij \rangle \rangle, \sigma} \hat{c}_{i\sigma}^{\dagger} \hat{c}_{j\sigma} + U \sum_{i} \hat{n}_{i\uparrow} \hat{n}_{i\downarrow}, (1)$$

where $\langle\langle ij\rangle\rangle$ denotes the next-nearest neighbor along the horizontal diagonal line with respect to the square lattice.

In these experiments, quantum gas microscope provides an in-situ, site-resolved imaging of the atomic distribution after a spin-selective removal of one component and in so doing measure the real-space magnetic correlation function

$$C_{r} = 4\left(\langle \hat{S}_{j}^{z} \hat{S}_{i}^{z} \rangle - \langle \hat{S}_{j}^{z} \rangle \langle \hat{S}_{i}^{z} \rangle\right), \tag{2}$$

where \mathbf{r} denotes the position of site-j relative to site-i and $\hat{S}_i^z = \frac{1}{2}(\hat{n}_{i\uparrow} - \hat{n}_{i\downarrow})$. A sample data of thus measured magnetic correlation from this quantum simulator is shown in Fig. 1(b).

TPSC and magnetic correlations.—For completeness, we review the basic ideas of TPSC using the Luttinger-Ward functional formalism [27]. In this formalism, the self-energy $\Sigma_{\sigma}[G_{\sigma}]$ is treated as a functional of the single-particle Green's function G_{σ} . Once a specific ansatz for the self-energy is given by some conserving scheme, the single-particle Green's function is determined by Dyson's equation. Preceding from here, however, are two independent routes to obtaining the two-particle Green's functions. One is through Heisenberg equation of motion which relates the single-particle Green's function to the two-particle one. The other is through Bethe-Salpeter equation, which expresses the susceptibilities,

essentially the two-particle Green's function, in terms of the effective interactions (i.e., the irreducible vertices) $\Gamma_{\sigma\sigma'}=\delta\Sigma_{\sigma}/\delta G_{\sigma'}$. The central idea of TPSC is to enforce the consistency in the calculations of the two-particle Green's function on the choice of the variational self-energy ansatz.

TPSC adopts a simple Hartree-like ansatz for the self-energy which assumes momentum- and frequency-independent irreducible vertices $\Gamma_{\uparrow\uparrow}$ and $\Gamma_{\uparrow\downarrow}$. In terms of the spin vertex $\Gamma_{sp} \equiv \Gamma_{\uparrow\downarrow} - \Gamma_{\uparrow\uparrow}$, the single-particle Green's function is given by

$$G_{\sigma}^{(1)}(\mathbf{k}, i\omega_m) = \frac{1}{i\omega_m - (\epsilon_{\mathbf{k}} + n\Gamma_{sp}/2 - \mu)}$$
(3)

where $\omega_m = (2m+1)\pi T$ is the fermonic Matsubara frequency at temperature T, $\epsilon_{\mathbf{k}} = -2t(\cos k_x + \cos k_y) - 2t'\cos(k_x + k_y)$ is the single-particle dispersion, n is the density and μ is the chemical potential. The equation of motion for the single-particle Green's function gives the following relation between the spin vertex Γ_{sp} and the double occupancy $\langle \hat{n}_{i\uparrow} \hat{n}_{i\downarrow} \rangle$

$$\Gamma_{sp}\langle \hat{n}_{i\uparrow}\rangle \langle \hat{n}_{i\downarrow}\rangle = U\langle \hat{n}_{i\uparrow}\hat{n}_{i\downarrow}\rangle. \tag{4}$$

The Bethe-Salpeter equation, which determines the spin susceptibility, leads to another relation between them

$$\frac{T}{N} \sum_{\nu} \sum_{\mathbf{q}} \frac{\chi^{(1)}(\mathbf{q}, i\omega_{\nu})}{1 - \frac{1}{2} \Gamma_{sp} \chi^{(1)}(\mathbf{q}, i\omega_{\nu})} = n - 2\langle \hat{n}_{i\uparrow} \hat{n}_{i\downarrow} \rangle, \quad (5)$$

where N is the number of lattice sites, n is the density, $\omega_{\nu} = 2\nu\pi T$ is the bosonic Matsubara frequency and

$$\chi^{(1)} \equiv \frac{T}{N} \sum_{m k \sigma} G_{\sigma}^{(1)}(\mathbf{k}, i\omega_m) G_{\sigma}^{(1)}(\mathbf{k} + \mathbf{q}, i\omega_m + i\omega_\nu) \quad (6)$$

is the so-called polarization bubble. For the single-particle Green's function given in Eq. (3), the latter takes the form of the Lindhard function $\chi^{(1)}(\boldsymbol{q},i\omega_{\nu})=-\frac{2}{N}\sum_{\boldsymbol{k}}\frac{f(\tilde{\epsilon}_{\boldsymbol{k}})-f(\tilde{\epsilon}_{\boldsymbol{k}+\boldsymbol{q}})}{i\omega_{\nu}+\tilde{\epsilon}_{\boldsymbol{k}}-\tilde{\epsilon}_{\boldsymbol{k}+\boldsymbol{q}}}$, where $\tilde{\epsilon}_{\boldsymbol{k}}=\epsilon_{\boldsymbol{k}}+n\Gamma_{sp}/2$ and $f(\tilde{\epsilon}_{\boldsymbol{k}})=1/(e^{(\tilde{\epsilon}_{\boldsymbol{k}}-\mu)/T}+1)$ is the Fermi-Dirac distribution.

To obtain the relation in Eq. (5), one first notes that the spin susceptibility can be obtained from the Bethe-Salpeter equation as

$$\chi_{sp}(\boldsymbol{q}, i\omega_{\nu}) = \frac{\chi^{(1)}(\boldsymbol{q}, i\omega_{\nu})}{1 - \frac{1}{2}\Gamma_{sp}\chi^{(1)}(\boldsymbol{q}, i\omega_{\nu})},$$
(7)

which in turn determines the spin structure factor

$$\tilde{C}_{\boldsymbol{q}} = T \sum_{\nu} \chi_{sp}(\boldsymbol{q}, i\omega_{\nu}). \tag{8}$$

Using the latter to calculate the real-space magnetic correlation function

$$C_{r} = \frac{1}{N} \sum_{\mathbf{q}} \tilde{C}_{\mathbf{q}} e^{i\mathbf{q} \cdot \mathbf{r}} \tag{9}$$

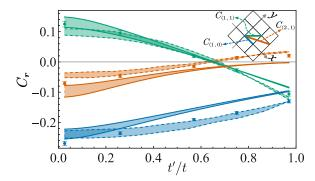


FIG. 2. The real-space magnetic correlation C_r between the nearest-, next-nearest and next-next-nearest neighbors, denoted by $C_{(1,0)}$, $C_{(1,1)}$ and $C_{(2,1)}$ respectively. For reference, $C_{(1,0)}=-1$ for a perfect antiferromagnetic Néel order. The dots with error bars are experimental data, the shaded bands with solid line boundaries are TPSC calculations and those with dashed lines are DQMC simulations. Here U/t=9.5, $T/t=0.3\sim0.35$ and n=1.

and observing that $C_{r=0} = n - 2\langle \hat{n}_{i\uparrow} \hat{n}_{i\downarrow} \rangle$, one arrives at Eq. (5). Once Γ_{sp} is determined self-consistently by solving Eqs. (4)-(5), the spin structure factor in Eq. (8) and the real-space magnetic correlation function in Eq. (9) can then be compared to experimental measurements. Lastly, we point out that the complete theory of TPSC involves additional steps to obtain a more accurate single-particle Green's function, but we omit this discussion as it is not relevant to our present purpose.

Benchmarking.—We first compare the magnetic correlations calculated by TPSC to those measured in the quantum simulator in the case of half-filling. To reaffirm the faithfulness of the quantum simulator we also perform determinant quantum Monte Carlo (DQMC) simulations [45] and include the results in the benchmarking. All TPSC calculations are done on a 256×256 lattice, where sparse sampling and IR decomposition from the sparse-ir library are used to treat the temperature Green's functions [46–48]. As mentioned earlier, the experiments measure directly the real-space correlation function C_r between any two sites. Shown in Fig. 2 are comparisons between theory and experiment on the nearest-, next-nearest and next-next-nearest neighbor correlations as a function of t'/t at U/t = 9.5. As the final temperature of the atomic system varies slightly from one value of t'/t to another, we show TPSC calculations (shaded bands in Fig. 2) for a range of temperatures $T/t = 0.3 \sim 0.35$, consistent with that determined in the experiments. We note that these temperatures are slightly lower than the spin exchange energy $J = 4t^2/U$. As we can see, the overall agreement between experiment and theory is excellent. At half-filling, the suppression of antiferromagnetic correlation by increasing frustration is clearly reflected by the reduction of the spin vertex in the TPSC calculations as shown in Fig. 3. However, we notice that the performance of TPSC declines slightly as frustration increases; in particular, the next-next-nearest

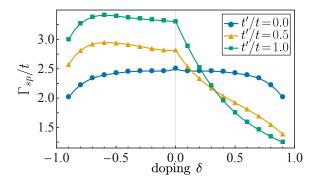


FIG. 3. The spin vertex Γ_{sp} as a function of doping at various degrees of frustration characterized by t'/t. Here U/t = 9.5, T/t = 0.35 and n = 1.

neighbor correlation $C_{(2,1)}$ does not turn positive for large t'/t as observed both in the quantum simulator and in DQMC.

In Ref. [14], the measured real-space magnetic correlations between all sites are then used to construct the spin structure factor \hat{C}_{q} by inverting Eq. (9). There, to illustrate clearly the effects of frustration, the physical lattice in Fig. 1 is mapped to a triangular lattice such that the square-shaped first Brillouin zone of the physical lattice now stretches into the rhombus-shaped one as illustrated in Fig. 4(a). Plotted as a function of the crystal momentum corresponding to the triangular lattice, the experimental $\tilde{C}_{\boldsymbol{q}}$ and the TPSC calculations are shown in Fig. 4. Here the TPSC reproduces the full spin structure factor of the Hubbard model simulator reasonably well; in particular, the splitting of the C_q peak at the M point into two parts at the K points as the frustration increases is well captured by the TPSC. We note that TPSC does produce a smaller peak value of the spin structure factor in general compared to the experimental measurements, which could be due to the limitation of the theory. Another possible explanation is that because of the system's non-uniform density the experimental determination of the spin structure factor involves a cutoff of real-space correlations beyond a certain distance, which may result in a less accurate peak value [49]. This truncation might also account for why the spin structure factor from the quantum simulator does not display additional oscillations as shown by TPSC (see Fig. 4(1)) [45].

We next consider the case of finite doping where the particle density is given by $n=1+\delta$. The comparisons between the TPSC calculations and the experimental results on the nearest and next-nearest neighbor correlations as a function of doping are shown in Fig. 5; again the agreements are on the whole very good. Here an important characteristic of frustrated lattices is the lack of particle-hole symmetry in contrast to the square lattice. This can be seen from the fact that the system with particle doping $\delta>0$ can be mapped to one with hole doping $-\delta$ and described by the same Hamiltonian with t' replaced by -t' [50–52]. In fact, the magnetic correlations

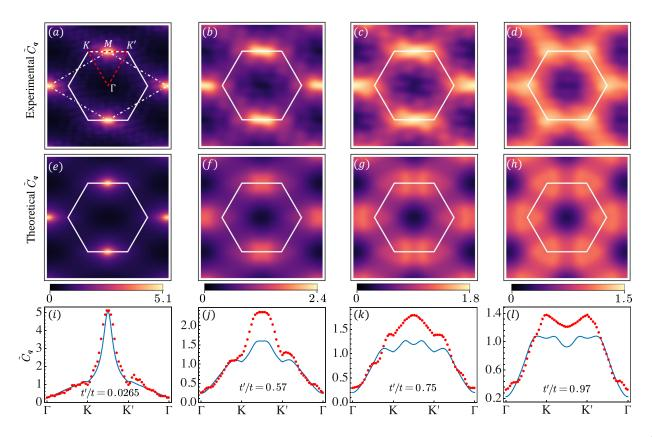


FIG. 4. Spin structure factor of the Hubbard model at half-filling and in increasing degree of frustration characterized by t'/t. The top panel contains results from the quantum simulator, the middle panel calculations from the TPSC and the bottom panel comparisons between them. The dots in the bottom panel are experimental data and lines TPSC calculations. Here experimental parameters corresponding to different t'/t are T/t = 0.26 and U/t = 9.7 for t'/t = 0.0265; T/t = 0.34 and U/t = 8.2 for t'/t = 0.57; T/t = 0.32 and U/t = 8.2 for t'/t = 0.75; and T/t = 0.39 and T/t = 0.39 and T/t = 0.39. All the TPSC calculations in the paper are done using experimental parameters except for the case of T/t = 0.0265, where we find an almost perfect agreement with the experiment using a theoretical T/t = 0.39.

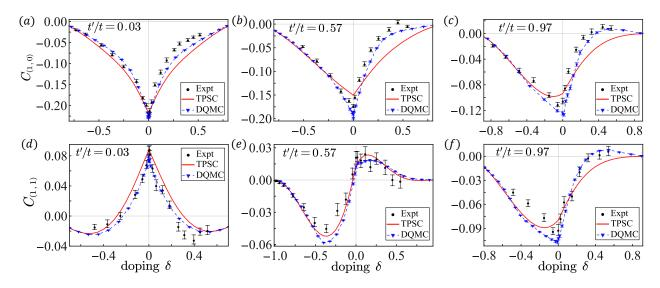


FIG. 5. The nearest- and next-nearest-neighbor correlations, $C_{(1,0)}$ and $C_{(1,1)}$, as a function of doping and at various degrees of frustration characterized by t'/t. Here the parameters used in our calculations are U/t = 9, and T/t = 0.35 for (a)-(c) and T/t = 0.4 for (d)-(f).

with particle doping are calculated using this mapping. The observed particle-hole asymmetry in frustrated lat-

tices is well captured by the TPSC calculations and, from the theoretical perspective, is due to the reduction of the spin vertex by particle doping in the presence of frustration (see Fig. 3). We notice that the experimental results in Fig. 5(c) has a somewhat more pronounced particlehole asymmetry than those of the TPSC calculations. In particular, the agreement between theory and experiment is almost perfect for the hole doping while some discrepancy exists for the particle doping. However, this discrepancy is perhaps not as large as it appears if we take into account the fact that the experimental results for the square lattice already exhibit a slight but noticeable particle-hole asymmetry (see Fig. 5(a)), due presumably to system errors. Nevertheless, the comparison in Fig. 5(c) clearly shows that TPSC does not capture the ferromagnetic correlations observed for the isotropic triangular lattice in the vicinity of particle doping $\delta = 1/2$. This may be an indication that the assumption of constant effective interactions from TPSC is not adequate here. Since in this case a van Hove singularity exists at the Fermi level in the density of states of the noninteracting system, any momentum dependence of the effective interactions will be accentuated by the presence of this singularity and can no longer be neglected [45].

Conclusions.—We have systematically benchmarked the TPSC calculations of the magnetic correlations of a doped and frustrated Hubbard model against the experimental results of a quantum simulator for $U/t = 8 \sim 10$. Although TPSC is believed to be valid only for weak-tointermediate coupling, i.e., for $U/t \lesssim 8$, the overall excellent agreement with the copious data from the quantum simulator indicates a wider range of applicability for this theory. In the future, it would be highly desirable to test other predictions of the TPSC, such as the opening of the pseudogap, in the next-generation of quantum simulators of the Hubbard model where the temperature can be further lowered. This can in principle be carried out by probing the single-particle spectral weight of the atomic system using the photoemission spectroscopy [53–55], a tool analogous to the ARPES in solid-state systems [56].

Acknowledgement. We are grateful to Dr. Muqing Xu and Prof. Markus Greiner for providing us the experimental data in Ref. [14]. We also want to thank Dr. Muqing Xu and Dr. Lev Kendrick for stimulating discussions. This work is supported by National Key R&D Program of China (Grant No. 2022YFA1404103), NSFC (Grant No. 11974161) and Shenzhen Science and Technology Program (Grant No. KQTD20200820113010023).

- [1] C. Gross and I. Bloch, Quantum simulations with ultracold atoms in optical lattices, Science **357**, 995 (2017).
- [2] L. Tarruell and L. Sanchez-Palencia, Quantum simulation of the hubbard model with ultracold fermions in optical lattices, Comptes Rendus Physique 19, 365 (2018).
- [3] A. Bohrdt, L. Homeier, C. Reinmoser, E. Demler, and F. Grusdt, Exploration of doped quantum magnets with ultracold atoms, Annals of Physics 435, 168651 (2021).
- [4] T. Esslinger, Fermi-hubbard physics with atoms in an optical lattice, Annual Review of Condensed Matter Physics 1, 129 (2010).
- [5] S. Kuhr, Quantum-gas microscopes: a new tool for coldatom quantum simulators, National Science Review 3, 170 (2016).
- [6] F. Schäfer, T. Fukuhara, S. Sugawa, Y. Takasu, and Y. Takahashi, Tools for quantum simulation with ultracold atoms in optical lattices, Nature Reviews Physics 2, 411 (2020).
- [7] T.-L. Ho and Q. Zhou, Squeezing out the entropy of fermions in optical lattices, Proceedings of the National Academy of Sciences 106, 6916 (2009).
- [8] J.-S. Bernier, C. Kollath, A. Georges, L. De Leo, F. Gerbier, C. Salomon, and M. Köhl, Cooling fermionic atoms in optical lattices by shaping the confinement, Phys. Rev. A 79, 061601 (2009).
- [9] D. Greif, M. F. Parsons, A. Mazurenko, C. S. Chiu, S. Blatt, F. Huber, G. Ji, and M. Greiner, Site-resolved imaging of a fermionic mott insulator, Science 351, 953 (2016).
- [10] L. W. Cheuk, M. A. Nichols, K. R. Lawrence, M. Okan, H. Zhang, E. Khatami, N. Trivedi, T. Paiva, M. Rigol, and M. W. Zwierlein, Observation of spatial charge and spin correlations in the 2d fermi-hubbard model, Science

- **353**, 1260 (2016).
- [11] A. Mazurenko, C. S. Chiu, G. Ji, M. F. Parsons, M. Kanász-Nagy, R. Schmidt, F. Grusdt, E. Demler, D. Greif, and M. Greiner, A cold-atom fermi-hubbard antiferromagnet, Nature 545, 462 (2017).
- [12] J. H. Drewes, L. A. Miller, E. Cocchi, C. F. Chan, N. Wurz, M. Gall, D. Pertot, F. Brennecke, and M. Köhl, Antiferromagnetic correlations in two-dimensional fermionic mott-insulating and metallic phases, Phys. Rev. Lett. 118, 170401 (2017).
- [13] P. T. Brown, D. Mitra, E. Guardado-Sanchez, P. Schauß, S. S. Kondov, E. Khatami, T. Paiva, N. Trivedi, D. A. Huse, and W. S. Bakr, Spin-imbalance in a 2d fermihubbard system, Science 357, 1385 (2017).
- [14] M. Xu, L. H. Kendrick, A. Kale, Y. Gang, G. Ji, R. T. Scalettar, M. Lebrat, and M. Greiner, Frustration- and doping-induced magnetism in a fermi-hubbard simulator, Nature 620, 971 (2023).
- [15] E. Cocchi, L. A. Miller, J. H. Drewes, M. Koschorreck, D. Pertot, F. Brennecke, and M. Köhl, Equation of state of the two-dimensional hubbard model, Phys. Rev. Lett. 116, 175301 (2016).
- [16] T. Hartke, B. Oreg, N. Jia, and M. Zwierlein, Doublon-hole correlations and fluctuation thermometry in a fermi-hubbard gas, Phys. Rev. Lett. 125, 113601 (2020).
- [17] J. Koepsell, J. Vijayan, P. Sompet, F. Grusdt, T. A. Hilker, E. Demler, G. Salomon, I. Bloch, and C. Gross, Imaging magnetic polarons in the doped fermi-hubbard model, Nature 572, 358 (2019).
- [18] J. Koepsell, D. Bourgund, P. Sompet, S. Hirthe, A. Bohrdt, Y. Wang, F. Grusdt, E. Demler, G. Salomon, C. Gross, and I. Bloch, Microscopic evolution of doped mott insulators from polaronic metal to fermi liquid, Sci-

- ence **374**, 82 (2021).
- [19] G. Ji, M. Xu, L. H. Kendrick, C. S. Chiu, J. C. Brüggenjürgen, D. Greif, A. Bohrdt, F. Grusdt, E. Demler, M. Lebrat, and M. Greiner, Coupling a mobile hole to an antiferromagnetic spin background: Transient dynamics of a magnetic polaron, Phys. Rev. X 11, 021022 (2021).
- [20] P. T. Brown, D. Mitra, E. Guardado-Sanchez, R. Nourafkan, A. Reymbaut, C.-D. Hébert, S. Bergeron, A.-M. S. Tremblay, J. Kokalj, D. A. Huse, P. Schauß, and W. S. Bakr, Bad metallic transport in a cold atom fermi-hubbard system, Science 363, 379 (2019).
- [21] M. A. Nichols, L. W. Cheuk, M. Okan, T. R. Hartke, E. Mendez, T. Senthil, E. Khatami, H. Zhang, and M. W. Zwierlein, Spin transport in a mott insulator of ultracold fermions, Science 363, 383 (2019).
- [22] E. Guardado-Sanchez, A. Morningstar, B. M. Spar, P. T. Brown, D. A. Huse, and W. S. Bakr, Subdiffusion and heat transport in a tilted two-dimensional fermi-hubbard system, Phys. Rev. X 10, 011042 (2020).
- [23] D. P. Arovas, E. Berg, S. A. Kivelson, and S. Raghu, The hubbard model, Annual Review of Condensed Matter Physics 13, 239 (2022).
- [24] T. Schäfer, N. Wentzell, F. Šimkovic, Y.-Y. He, C. Hille, M. Klett, C. J. Eckhardt, B. Arzhang, V. Harkov, F. m. c.-M. Le Régent, A. Kirsch, Y. Wang, A. J. Kim, E. Kozik, E. A. Stepanov, A. Kauch, S. Andergassen, P. Hansmann, D. Rohe, Y. M. Vilk, J. P. F. LeBlanc, S. Zhang, A.-M. S. Tremblay, M. Ferrero, O. Parcollet, and A. Georges, Tracking the footprints of spin fluctuations: A multimethod, multimessenger study of the two-dimensional hubbard model, Phys. Rev. X 11, 011058 (2021).
- [25] M. Qin, T. Schäfer, S. Andergassen, P. Corboz, and E. Gull, The hubbard model: A computational perspective, Annual Review of Condensed Matter Physics 13, 275 (2022).
- [26] Y. M. Vilk and A.-M. Tremblay, Non-perturbative manybody approach to the hubbard model and single-particle pseudogap, Journal de Physique I 7, 1309 (1997).
- [27] A.-M. S. Tremblay, Two-particle-self-consistent approach for the hubbard model, in *Springer Series in Solid-State Sciences* (Springer Berlin Heidelberg, 2011) pp. 409–453.
- [28] T. Saikawa and A. Ferraz, Remnant fermi surface in a pseudogap regime of the two-dimensional hubbard model at finite temperature, The European Physical Journal B - Condensed Matter and Complex Systems 20, 65 (2001).
- [29] V. Hankevych, B. Kyung, and A.-M. S. Tremblay, Weak ferromagnetism and other instabilities of the two-dimensional $t-t^{'}$ hubbard model at van hove fillings, Phys. Rev. B **68**, 214405 (2003).
- [30] B. Kyung, J.-S. Landry, and A.-M. S. Tremblay, Antiferromagnetic fluctuations and d-wave superconductivity in electron-doped high-temperature superconductors, Phys. Rev. B 68, 174502 (2003).
- [31] B. Kyung, V. Hankevych, A.-M. Daré, and A.-M. S. Tremblay, Pseudogap and spin fluctuations in the normal state of the electron-doped cuprates, Phys. Rev. Lett. 93, 147004 (2004).
- [32] A.-M. S. Tremblay, B. Kyung, and D. Sénéchal, Pseudogap and high-temperature superconductivity from weak to strong coupling. Towards a quantitative theory (Review Article), Low Temperature Physics 32, 424 (2006).

- [33] V. Hankevych, B. Kyung, A.-M. Daré, D. Sénéchal, and A.-M. Tremblay, Strong- and weak-coupling mechanisms for pseudogap in electron-doped cuprates, Journal of Physics and Chemistry of Solids 67, 189 (2006).
- [34] B. Davoudi and A.-M. S. Tremblay, Nearest-neighbor repulsion and competing charge and spin order in the extended hubbard model, Phys. Rev. B 74, 035113 (2006).
- [35] A.-M. Daré, L. Raymond, G. Albinet, and A.-M. S. Tremblay, Interaction-induced adiabatic cooling for antiferromagnetism in optical lattices, Phys. Rev. B 76, 064402 (2007).
- [36] S. R. Hassan, B. Davoudi, B. Kyung, and A.-M. S. Tremblay, Conditions for magnetically induced singlet d-wave superconductivity on the square lattice, Phys. Rev. B 77, 094501 (2008).
- [37] D. Bergeron, V. Hankevych, B. Kyung, and A.-M. S. Tremblay, Optical and dc conductivity of the twodimensional hubbard model in the pseudogap regime and across the antiferromagnetic quantum critical point including vertex corrections, Phys. Rev. B 84, 085128 (2011).
- [38] J. Otsuki, Two-particle self-consistent approach to unconventional superconductivity, Phys. Rev. B 85, 104513 (2012).
- [39] S. Arya, P. V. Sriluckshmy, S. R. Hassan, and A.-M. S. Tremblay, Antiferromagnetism in the hubbard model on the honeycomb lattice: A two-particle self-consistent study, Phys. Rev. B 92, 045111 (2015).
- [40] K. Nishiguchi, S. Teranishi, K. Kusakabe, and H. Aoki, Superconductivity arising from layer differentiation in multilayer cuprates, Phys. Rev. B 98, 174508 (2018).
- [41] K. Zantout, S. Backes, and R. Valentí, Two-particle selfconsistent method for the multi-orbital hubbard model, Annalen der Physik 533, 2000399 (2021).
- [42] N. Martin, C. Gauvin-Ndiaye, and A.-M. S. Tremblay, Nonlocal corrections to dynamical mean-field theory from the two-particle self-consistent method, Phys. Rev. B 107, 075158 (2023).
- [43] D. Lessnich, C. Gauvin-Ndiaye, R. Valentí, and A. M. S. Tremblay, Spin hall conductivity in the kane-mele-hubbard model at finite temperature (2023), arXiv:2307.15652 [cond-mat.str-el].
- [44] C. Gauvin-Ndiaye, J. Leblanc, S. Marin, N. Martin, D. Lessnich, and A.-M. S. Tremblay, Two-particle selfconsistent approach for multiorbital models: Application to the emery model, Phys. Rev. B 109, 165111 (2024).
- [45] See Supplemental Material for more details on the determinant quantum Monte Carlo simulation, the spin structure factor and the ferromagnetic correlations, which includes Ref. [57] and Ref. [58].
- [46] H. Shinaoka, J. Otsuki, M. Ohzeki, and K. Yoshimi, Compressing green's function using intermediate representation between imaginary-time and real-frequency domains, Phys. Rev. B 96, 035147 (2017).
- [47] J. Li, M. Wallerberger, N. Chikano, C.-N. Yeh, E. Gull, and H. Shinaoka, Sparse sampling approach to efficient ab initio calculations at finite temperature, Phys. Rev. B 101, 035144 (2020).
- [48] M. Wallerberger, S. Badr, S. Hoshino, S. Huber, F. Kakizawa, T. Koretsune, Y. Nagai, K. Nogaki, T. Nomoto, H. Mori, J. Otsuki, S. Ozaki, T. Plaikner, R. Sakurai, C. Vogel, N. Witt, K. Yoshimi, and H. Shinaoka, sparseir: Optimal compression and sparse sampling of manybody propagators, SoftwareX 21, 101266 (2023).

- [49] Muqing Xu, private communications.
- [50] C. Li, M.-G. He, C.-Y. Wang, and H. Zhai, Frustrationinduced itinerant ferromagnetism of fermions in optical lattices, Phys. Rev. B 109, 165131 (2024).
- [51] R. Samajdar and R. N. Bhatt, Nagaoka ferromagnetism in doped hubbard models in optical lattices (2023), arXiv:2305.05683 [cond-mat.str-el].
- [52] R. Samajdar and R. N. Bhatt, Polaronic mechanism of nagaoka ferromagnetism in hubbard models (2023), arXiv:2311.09279 [cond-mat.str-el].
- [53] T.-L. Dao, A. Georges, J. Dalibard, C. Salomon, and I. Carusotto, Measuring the one-particle excitations of ultracold fermionic atoms by stimulated raman spectroscopy, Phys. Rev. Lett. 98, 240402 (2007).
- [54] J. T. Stewart, J. P. Gaebler, and D. S. Jin, Using photoemission spectroscopy to probe a strongly interacting

- fermi gas, Nature 454, 744 (2008).
- [55] J. P. Gaebler, J. T. Stewart, T. E. Drake, D. S. Jin, A. Perali, P. Pieri, and G. C. Strinati, Observation of pseudogap behaviour in a strongly interacting fermi gas, Nature Physics 6, 569 (2010).
- [56] A. Damascelli, Z. Hussain, and Z.-X. Shen, Angleresolved photoemission studies of the cuprate superconductors, Rev. Mod. Phys. 75, 473 (2003).
- [57] J. Gubernatis, N. Kawashima, and P. Werner, Quantum Monte Carlo Methods: Algorithms for Lattice Models (Cambridge University Press, 2016).
- [58] B. Cohen-Stead, S. M. Costa, J. Neuhaus, A. T. Ly, Y. Zhang, R. Scalettar, K. Barros, and S. Johnston, Smo-QyDQMC.jl: A flexible implementation of determinant quantum Monte Carlo for Hubbard and electron-phonon interactions, SciPost Phys. Codebases, 29 (2024).

Supplemental Material for "Magnetic correlations of a doped and frustrated Hubbard model: benchmarking the two-particle self-consistent theory against a quantum simulator"

Guan-Hua Huang¹ and Zhigang Wu^{2,*}

¹Hefei National Laboratory, Hefei 230088, China

²Quantum Science Center of Guangdong-Hong Kong-Macao Greater Bay Area (Guangdong), Shenzhen 508045, China

(Dated: September 6, 2024)

This supplemental material includes the following three sections: (I) Determinant quantum Monte Carlo simulation; (II) Spin structure factor and (III) Ferromagnetic correlations.

I. DETERMINANT QUANTUM MONTE CARLO SIMULATION

Determinant quantum Monte Carlo (DQMC) method, also known the auxiliary field quantum Monte Carlo method, is a finite-temperature algorithm developed for the simulation of models of interacting electrons on a lattice, such as the Hubbard model [1]. For the purpose of reaffirming the faithfulness of the quantum simulator in Ref. [2], we perform DQMC simulations for all the system parameters probed by the quantum simulator using the SmoQyDQMC.jl package [3]. The simulations are performed on an 8×8 lattice with the imaginary time Trotter step size $d\tau = \beta/N_{\tau} \approx 0.02/t$. As DQMC simulations encounter the negative sign problem at low temperatures in the frustrated Hubbard model, sufficient statistical averaging is needed to reduce the computation error. Specifically, for temperatures T/t = 0.3, we average over 40 independent runs with different seeds to obtain reliable statistics where each run is generated with 5000 warm-up passes and 30000 measurement passes; for temperatures T/t = 0.35, we average over 20 runs where each run is generated with 5000 warm-up passes and 15000 measurement passes.

^{*} atticuspku@gmail.com

II. SPIN STRUCTURE FACTOR

Experimentally, the spin structure factor is obtained by Fourier transforming the realspace spin correlation function C_r , i.e.,

$$\tilde{C}_{q} = \sum_{r}^{|r| \le d_{max}} C_{r} e^{iq \cdot r}, \tag{S1}$$

where the sum is truncated at a maximum distance d_{max} . Although the experiments measure real-space spin correlations up to a distance of d=11 (in units of lattice spacing), the experimental spin structure factor in Fig. S1(a) is obtained by taking $d_{max}=5$ (see Methods section of Ref. [2]). The reason is that experimentalists regard the measured real-space correlations beyond $d_{max}=5$ as noises [4] and thus discarded them. However, if we use the complete experimental data to compute the spin structure factor instead, we find a result shown in Fig. S1(b). Interestingly, this spin structure factor exhibits oscillations just like the TPSC results, although the peaks are more pronounced than those in TPSC. In our view, the existence of the additional oscillations from TPSC reflects the fact that the spin structure factor obtained using this approach contains contributions from long-distance spin correlations.

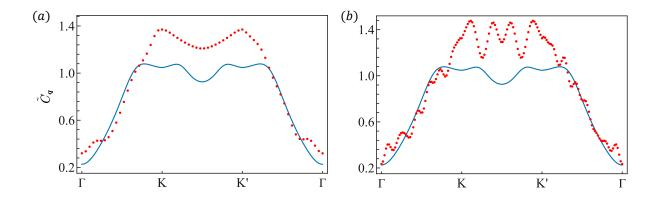


FIG. S1. (a) Comparison between the spin structure factor from TPSC (solid line) and that from the quantum simulator (dots) with truncated Fourier sum. (b) Comparison between the spin structure factor from TPSC (solid line) and that from the quantum simulator (dots) with complete Fourier sum.

III. FERROMAGNETIC CORRELATIONS

We have seen in the main text that TPSC fails to capture the ferromagnetic correlation observed in the quantum simulator for the triangular lattice in the vicinity of particle doping $\delta = 1/2$. As shown in Fig. S2(a) here, the nearest-neighbor correlation $C_{(1,0)}$ from the

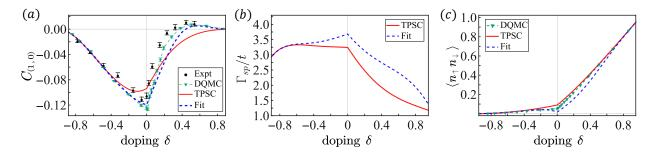


FIG. S2. (a) The nearest-neighbor correlation $C_{(1,0)}$ from TPSC, TPSC with a fitted Γ_{sp} shown in (b), the quantum simulator and DQMC. Here t'/t = 0.97, U/t = 9, and T/t = 0.35. (b) Γ_{sp} obtained from TPSC and Γ_{sp} that yields the dashed (blue) curve in (a). (c) The double occupancy obtained from TPSC, DQMC and the TPSC with a fitted Γ_{sp} .

quantum simulator and DQMC become positive at particle doping $\delta = 1/2$ for t'/t = 0.97 while the TPSC result does not. However, if we treat Γ_{sp} as a free fitting parameter in Eq. (7) of the main text, we can obtain ferromagnetic correlations at particle doping $\delta = 1/2$ by choosing appropriate Γ_{sp} values. For example, if we choose Γ_{sp} as indicated by the blue dashed line in Fig. S2(b), the resulting $C_{(1,0)}$ can actually capture the ferromagnetic correlation as shown in Fig S2(a). But this new Γ_{sp} leads to a double occupancy that deviates further away from the original TPSC and DQMC values as shown by Fig S2(c). This clearly shows the inadequacy of assuming a momentum and frequency independent Γ_{sp} in this case.

It is intriguing that the case of isotropic triangular lattice around particle doping of $\delta = 1/2$ is special in this sense. We postulate that it might be related to the fact that there is a van Hove singularity at Fermi level in the non-interacting density of states, which is shown in Fig. S3. To see this we first note that if we retain the momentum and frequency dependence of the spin vertex $\Gamma_{sp}(\mathbf{q}, i\omega_{\nu})$, the spin susceptibility is given by

$$\chi_{sp}(\boldsymbol{q}, i\omega_{\nu}) = \frac{\chi^{(1)}(\boldsymbol{q}, i\omega_{\nu})}{1 - \frac{1}{2}\Gamma_{sp}(\boldsymbol{q}, i\omega_{\nu})\chi^{(1)}(\boldsymbol{q}, i\omega_{\nu})},$$
 (S2)

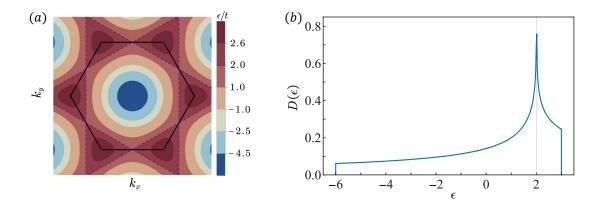


FIG. S3. (a) The first Brillouin zone of non-interacting band structure of the isotropic triangular lattice, where the dashed line shows the Fermi surface corresponding to particle doping at $\delta = 1/2$. (b) The density of states of the non-interacting band structure of the isotropic triangular lattice, where the van Hove singularity occurs at the Fermi level $\mu = 2t$.

from which the real-space magnetic correlation function can be determined as

$$C_{r} = \frac{T}{N} \sum_{\boldsymbol{q},\nu} \chi_{sp}(\boldsymbol{q}, i\omega_{\nu}) e^{i\boldsymbol{q}\cdot\boldsymbol{r}}$$

$$= \frac{T}{N} \sum_{\boldsymbol{q},\nu} \frac{\chi^{(1)}(\boldsymbol{q}, i\omega_{\nu})}{1 - \frac{1}{2} \Gamma_{sp}(\boldsymbol{q}, i\omega_{\nu}) \chi^{(1)}(\boldsymbol{q}, i\omega_{\nu})} e^{i\boldsymbol{q}\cdot\boldsymbol{r}}$$

$$= T \sum_{\nu} \int d\epsilon D(\epsilon) \frac{\chi^{(1)}(\boldsymbol{q}, i\omega_{\nu})}{1 - \frac{1}{2} \Gamma_{sp}(\boldsymbol{q}, i\omega_{\nu}) \chi^{(1)}(\boldsymbol{q}, i\omega_{\nu})} e^{i\boldsymbol{q}\cdot\boldsymbol{r}}, \tag{S3}$$

where $D(\epsilon)$ is the density of states of the non-interacting system. Since $\Gamma_{sp}(\mathbf{q}, i\omega_{\nu})$ depends on ϵ through \mathbf{q} , any momentum-dependence of $\Gamma_{sp}(\mathbf{q}, i\omega_{\nu})$ will be magnified by the presence of the singularity and can no longer be neglected. It would be an important goal for our future work to generalize TPSC further by including the momentum and frequency-dependence of the spin vertex in a way which does not violate the two-particle self-consistency.

^[1] J. Gubernatis, N. Kawashima, and P. Werner, Quantum Monte Carlo Methods: Algorithms for Lattice Models (Cambridge University Press, 2016).

^[2] M. Xu, L. H. Kendrick, A. Kale, Y. Gang, G. Ji, R. T. Scalettar, M. Lebrat, and M. Greiner, Frustration- and doping-induced magnetism in a fermi-hubbard simulator, Nature 620, 971 (2023).

- [3] B. Cohen-Stead, S. M. Costa, J. Neuhaus, A. T. Ly, Y. Zhang, R. Scalettar, K. Barros, and S. Johnston, SmoQyDQMC.jl: A flexible implementation of determinant quantum Monte Carlo for Hubbard and electron-phonon interactions, SciPost Phys. Codebases, 29 (2024).
- [4] Muqing Xu, private communications.